Supplementary Figures

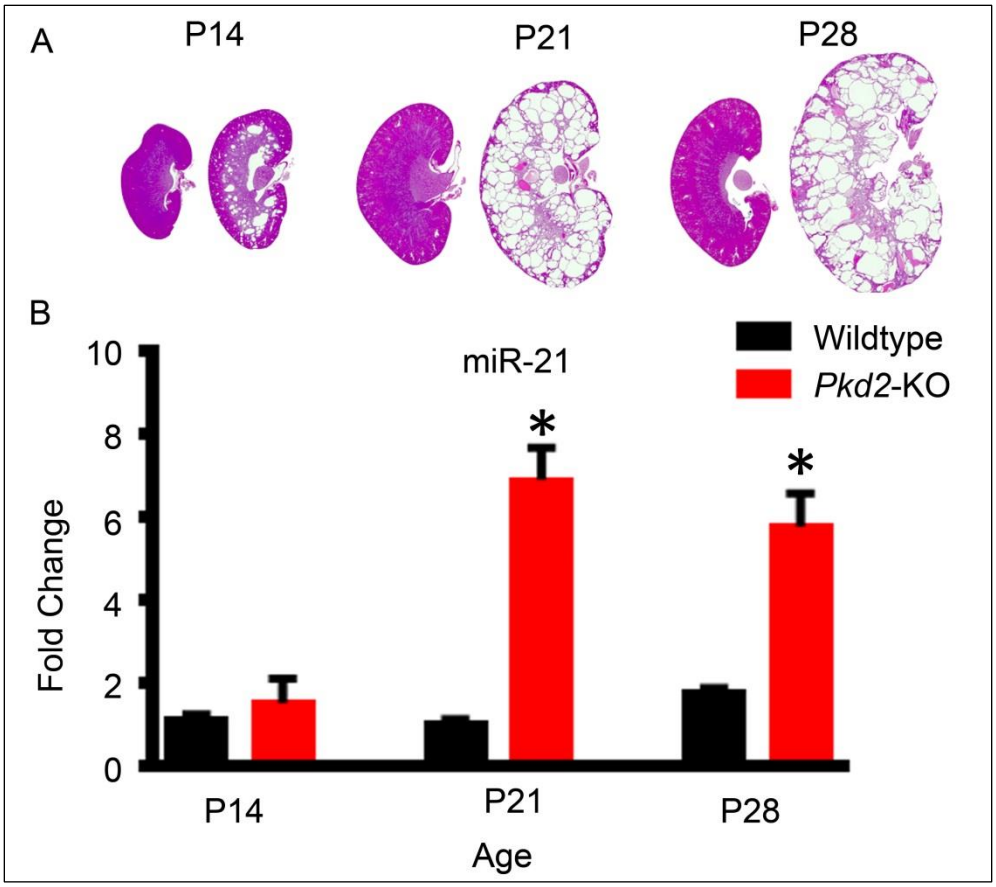

Supplementary Figure 1: Up-regulation of miR-21 expression corresponds with cyst expansion: (A) H&E sections of wild type and *Pkd2*-KO kidneys at postnatal days (P) 14, 21 and 28 is shown. All images were acquired under the same magnification. (B) Q-PCR analysis showed that the expression of miR-21 is upregulated at P21 and P28. There was no change in miR-21 expression at P14 indicating that miR-21 up-regulation is associated with cyst expansion rather than cyst initiation. N=3, *P<0.05, Error bars represent SEM.

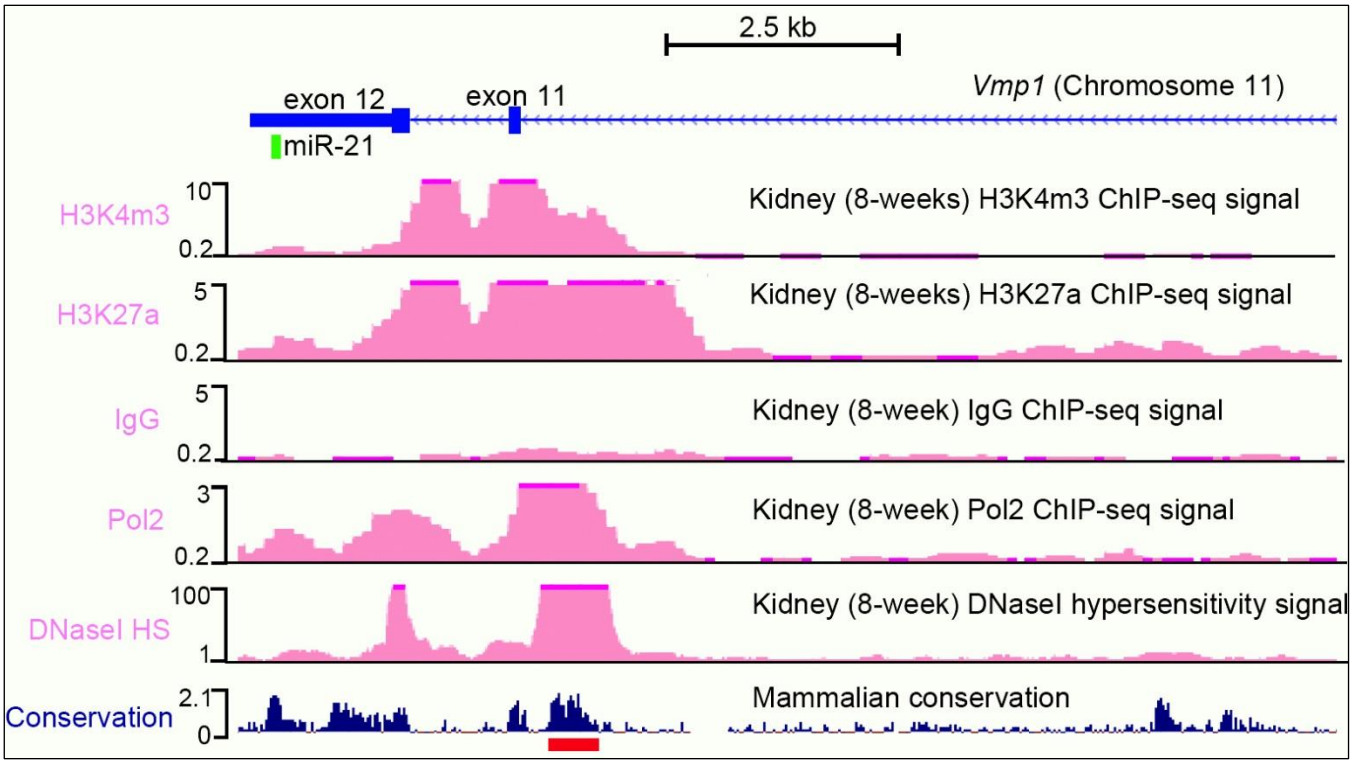

Supplementary Figure 2: miR-21 genomic organization and transcriptional regulation of the mouse miR-21 locus. In mice, miR-21 gene (green box) is located in exon 12 of *Vmp1* (blue box) (July 2007 assembly NCBI37/mm9, http://genome.ucsc.edu). Alignment of the human miR-21 promoter sequence (red box) with the mouse genome identified a 419 bp conserved region in intron 10 of *Vmp1*. Incorporation of data from the mouse ENCODE project revealed that intron 10 of *Vmp1* corresponds to marks of an active promoter in adult mouse kidney, including binding of RNA Polymerase 2, histone H3 lysine 4 tri-methylation (H3K4m3), histone H3 lysine 27 acetylation (H3K27a), and hypersensitivity (HS) to DNase I enzyme.

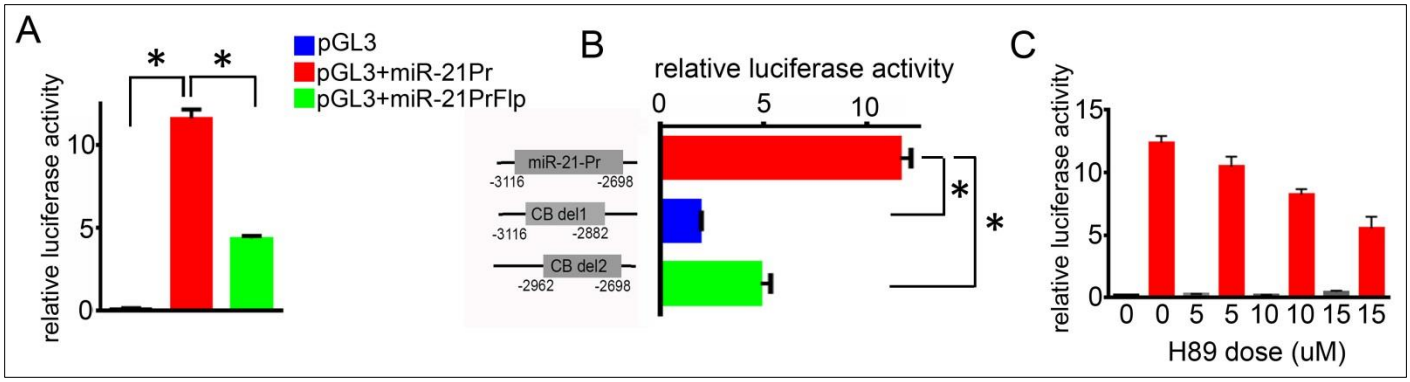

Supplementary Figure 3: miR-21 promoter is transcriptionally active in *Pkd2*$^{-/-}$ cells (A) Luciferase activity of pGL3+miR-21Pr and pGL3+miR-21PrFlp in *Pkd2*$^{-/-}$ cells is shown (N=6). (B) The activity of constructs in *Pkd2*$^{-/-}$ cells where CREB binding sites have been deleted (pGL3-CB-del1 and pGL3-CBdel2) compared to pGL3-miR-21-Pr is shown (N=6). (C) To assess the effect of PKA inhibition on the miR-21 promoter in *Pkd2*$^{-/-}$ cells, increasing doses of H89 were given to *Pkd2*$^{-/-}$ cells which had been transfected with pGL3-miR-21Pr (N=3). *P<0.05, Error bars represent SEM.

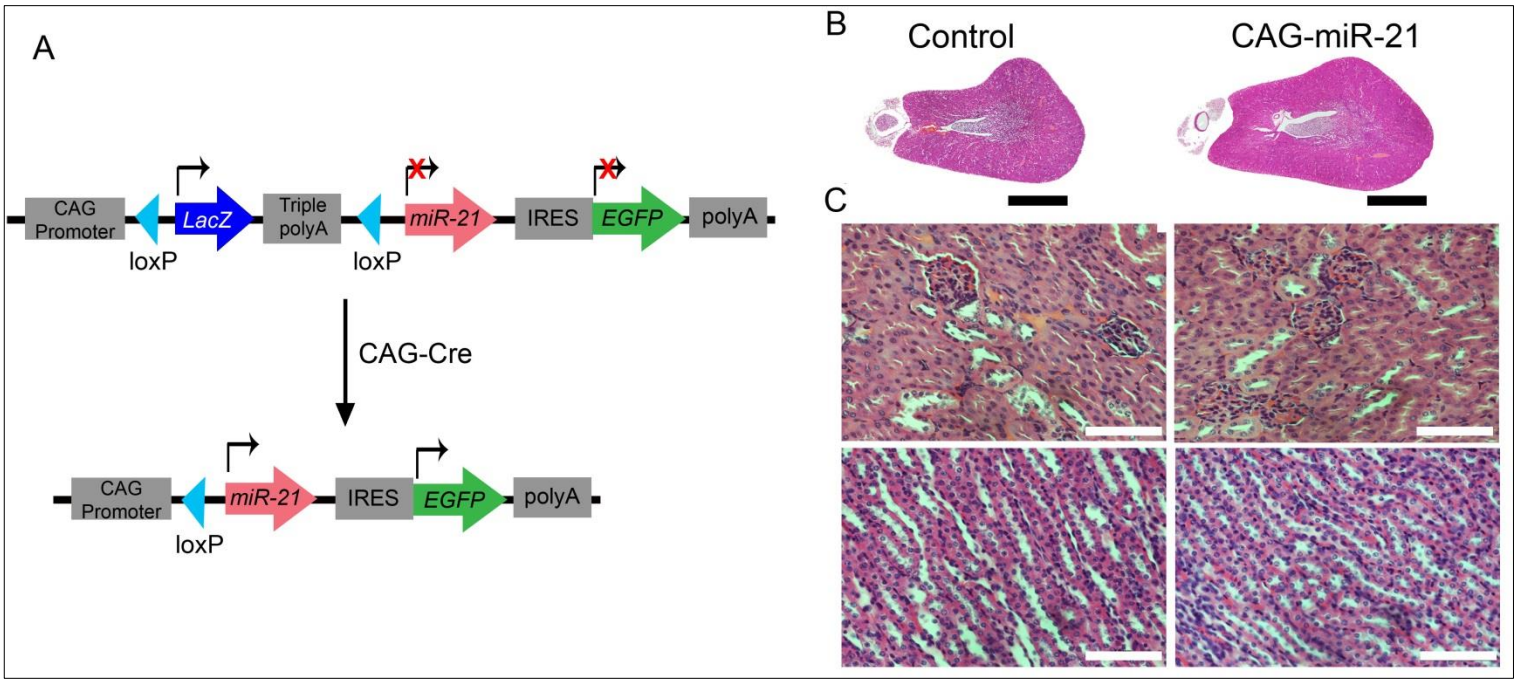

Supplementary Figure 4: miR-21 overexpression is not sufficient to produce kidney cysts. (A) The construct and the strategy used to generate CAG-miR-21 mice is shown. Kidney sections from 8-week-old control and CAG-miR-21 mice were stained with H&E. miR-21 is expressed 4 to 6-fold higher in CAG-miR-21 mice compared to control mice. (B) Low power and (C) 40x images of 8-week-old control and CAG-miR-21 transgenic mice are shown. No histological abnormalities were observed in CAG-miR-21 mice. Scale bars in A = 1000 µm and B = 50 µm.

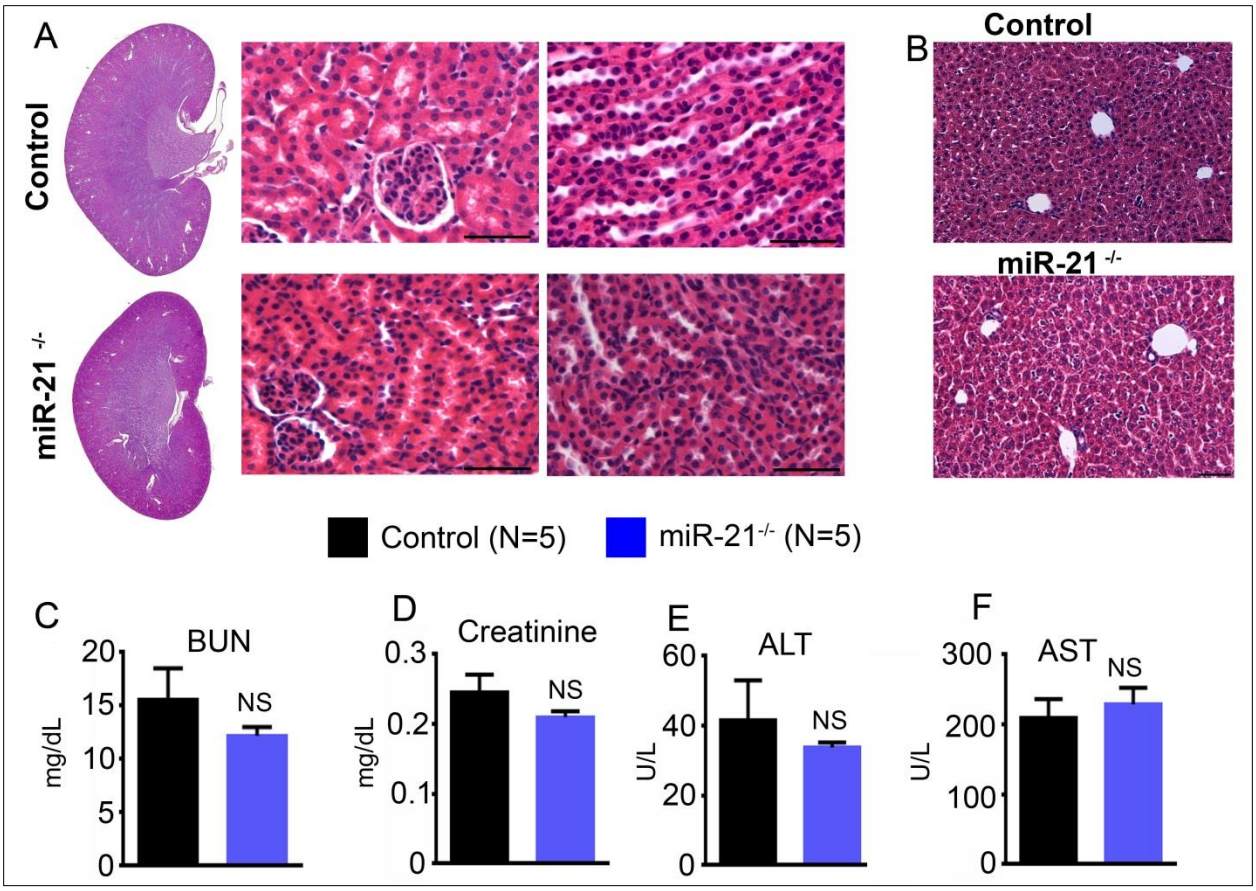

Supplementary Figure 5: Characterization of miR-21$^{-/-}$ mice. (A) Low power and 40x magnification images of H&E stained kidney sections of 21-day-old control and miR-21$^{-/-}$ mice are shown. No histological abnormalities were observed in kidneys of miR-21$^{-/-}$ mice. (B) 20x magnification images of H&E stained liver sections of 21-day-old control and miR-21 $^{-/-}$ mice are shown. No histological abnormalities were observed in the livers of miR-21$^{-/-}$ mice. Serum BUN (C), creatinine (D), ALT (E) and AST (F) levels of control and miR-21$^{-/-}$ also revealed no significant difference. NS indicates *P*>0.05, Error bars represent SEM. Scale bars represent 50 µm.

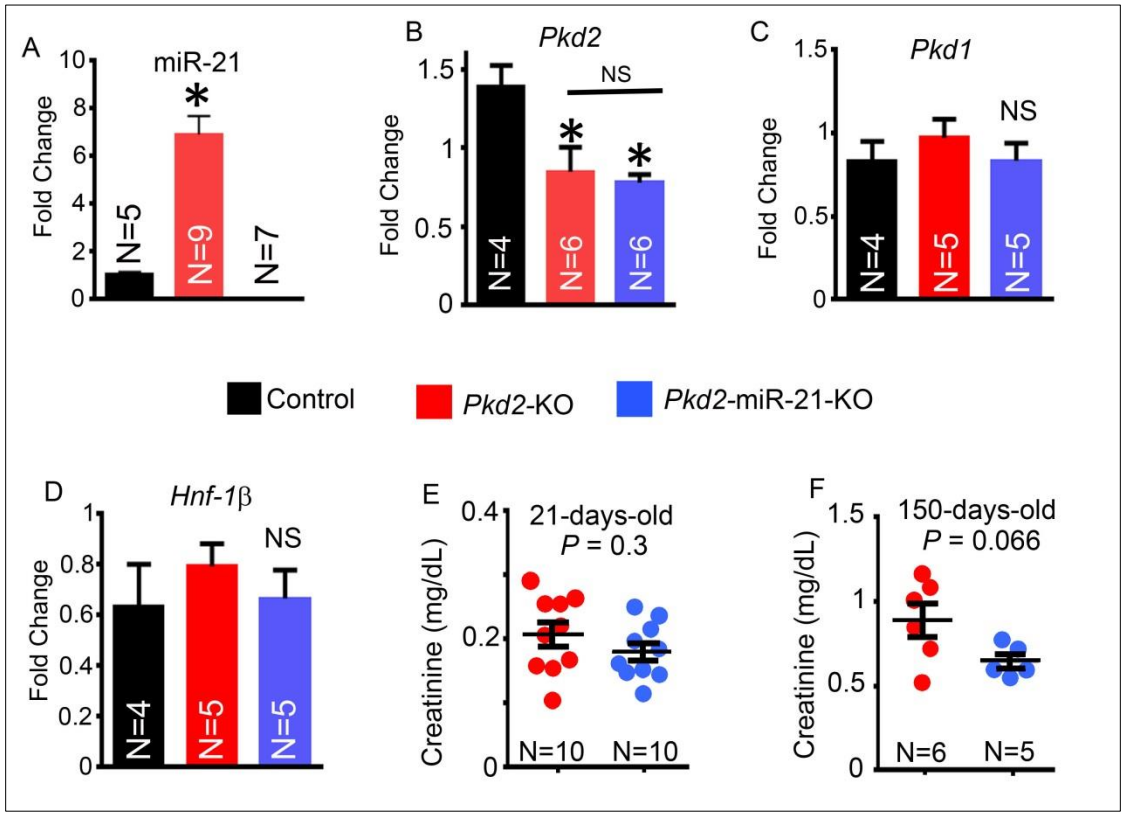

Supplementary Figure 6: Characterization of *Pkd2*-KO and *Pkd2*-miR-21-KO mice. (A) Q-PCR analysis showed that miR-21 is significantly upregulated in kidneys of *Pkd2*-KO mice compared to control mice, whereas its expression is abolished in kidneys of *Pkd2*-miR-21-KO mice. (B) *Pkd2* expression is equally reduced in kidneys of *Pkd2*-KO and *Pkd2*-miR-21-KO mice compared to control mice indicating that similar level of cre-loxP recombination efficiency was observed in *Pkd2*-KO and *Pkd2*-miR-21-KO mice. *Pkd1* (C) and *Hnf-1β* (D) expression was unchanged between control, *Pkd2*-KO and *Pkd2*-miR-21-KO mice. (E) Serum creatinine level was not different in 21-day-old *Pkd2*-miR-21-KO mice compared to *Pkd2*-KO mice ($P = 0.3$). (F) Serum creatinine level was numerically lower in 150-day-old *Pkd2*-miR-21-KO mice compared *Pkd2*-KO mice; however, this difference did not reach statistical significance (P =0.066). * $P<0.05$, NS $P>0.05$ Error bars represent SEM.

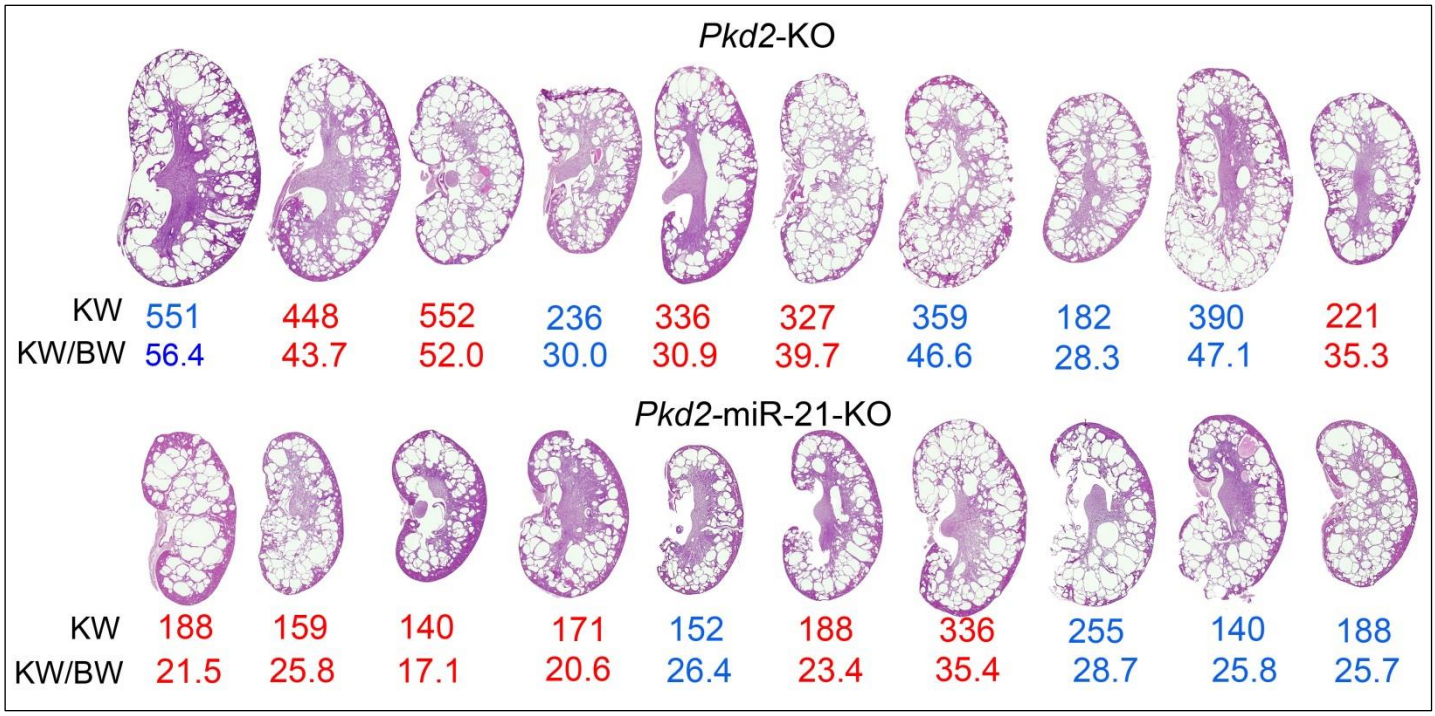

Supplementary Figure 7: Deletion of miR-21 attenuates cyst burden in *Pkd2*-KO mice. Ten pairs of 21-day-old *Pkd2*-KO mice and *Pkd2*-miR-21-KO mice were sacrificed to perform histological and molecular analysis shown in figure 3. H&E staining of kidney sections and associated kidney weights and kidney-weight-to-body-weight ratios for all mice analyzed for this study is shown. All images were acquired under the same magnification. Red font denotes male mice and blue font denotes female mice. No difference was observed between male and female mice.

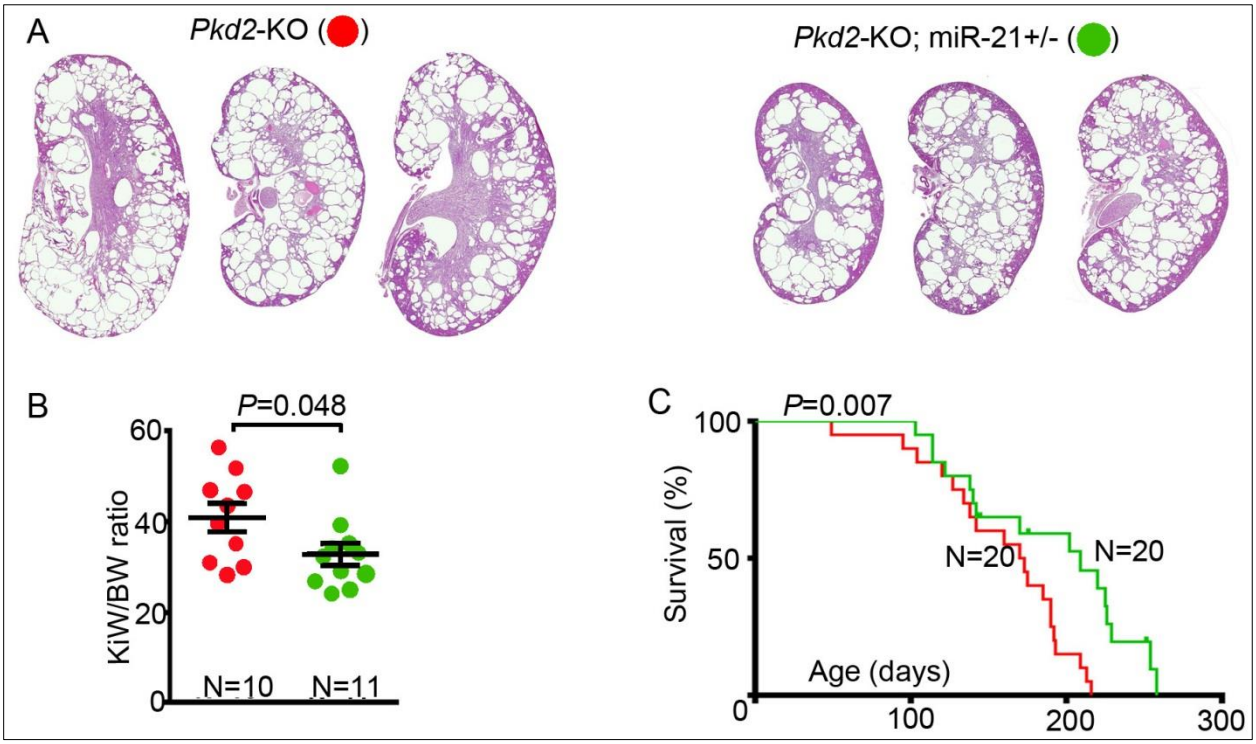

Supplementary Figure 8: Deletion of one allele of miR-21 is sufficient to reduce cyst burden and prolong survival. (A) Representative images of H&E stained kidney sections of three different *Pkd2*-KO mice and *Pkd2*-KO; miR-21$^{+/-}$ (*Pkd2*-miR-21-het-KO) is shown. (B) Kidney-weight-to-body-weight (KiW/BW) ratio was reduced in *Pkd2*-miR-21-het-KO (green) compared to *Pkd2*-KO (red) mice. (C) Kaplan-Meier survival curves of *Pkd2*-miR-21-het-KO (green line) and *Pkd2*-KO mice (red line). Error bars represent SEM.

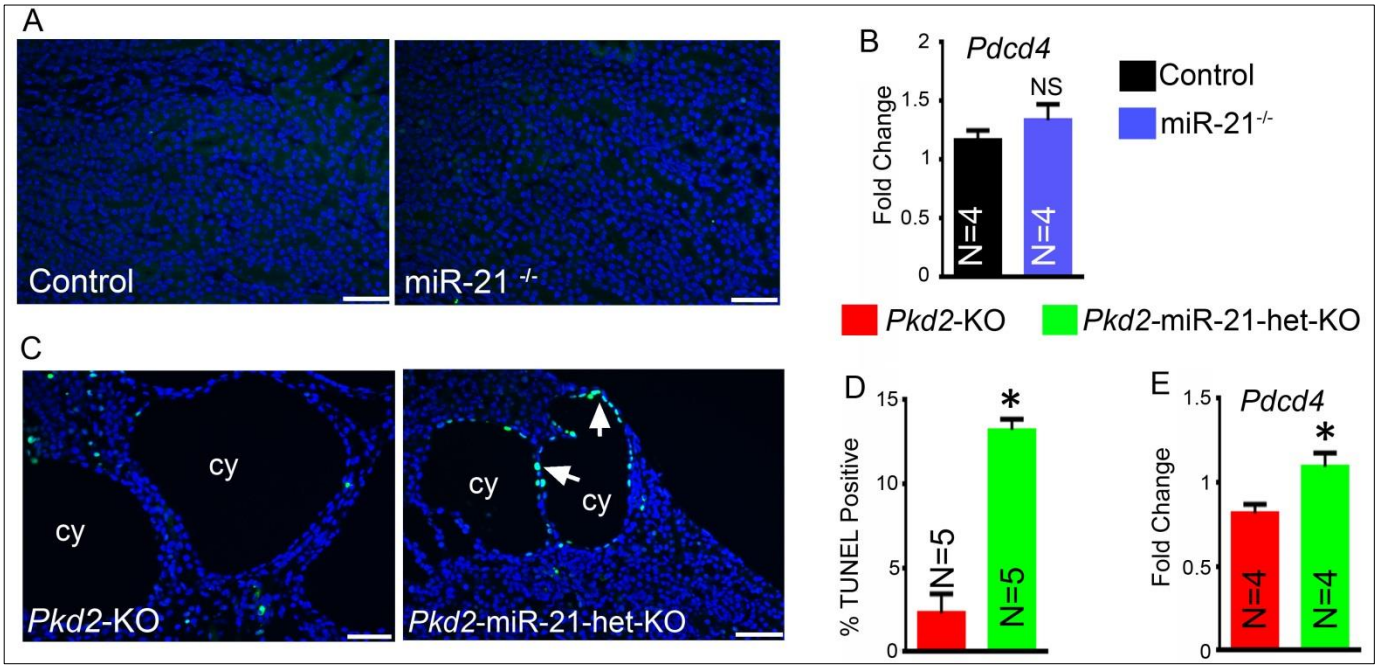

Supplementary Figure 9: Characterization of apoptosis and *Pdcd4* expression in mice with miR-21 deletion. (A) Kidney sections of 21-day-old control and miR-21$^{-/-}$ mice were stained using the TUNEL assay to detect kidney cells that were undergoing apoptosis. No apoptosis was observed in kidneys of control or miR-21$^{-/-}$ mice. (B) Q-PCR analysis showed that *Pdcd4* expression was unchanged in kidneys of miR-21$^{-/-}$ mice compared to control mice. (C) Kidney sections of 21-day-old *Pkd2*-KO and *Pkd2*-miR-21-het-KO mice were stained using the TUNEL assay to detect cyst epithelial cells that were undergoing apoptosis (green, white arrows). (D) Quantification revealed that cyst epithelial apoptosis was increased ~5-fold in *Pkd2*-miR-21-het-KO mice compared to *Pkd2*-KO mice. (E) Q-PCR analysis showed that *Pdcd4* expression was also increased in *Pkd2*-miR-21-het-KO mice compared to *Pkd2*-KO mice. Thus, deletion of miR-21 does not affect *Pdcd4* expression or evoke apoptosis of normal kidney cells. However, deletion of miR-21 in context of PKD is associated with increased apoptosis of cyst epithelial cells and up-regulation of *Pdcd4* expression. Scale bars indicate 50 μm. **P*<0.05, NS *P*>0.05, Error bars represent SEM.

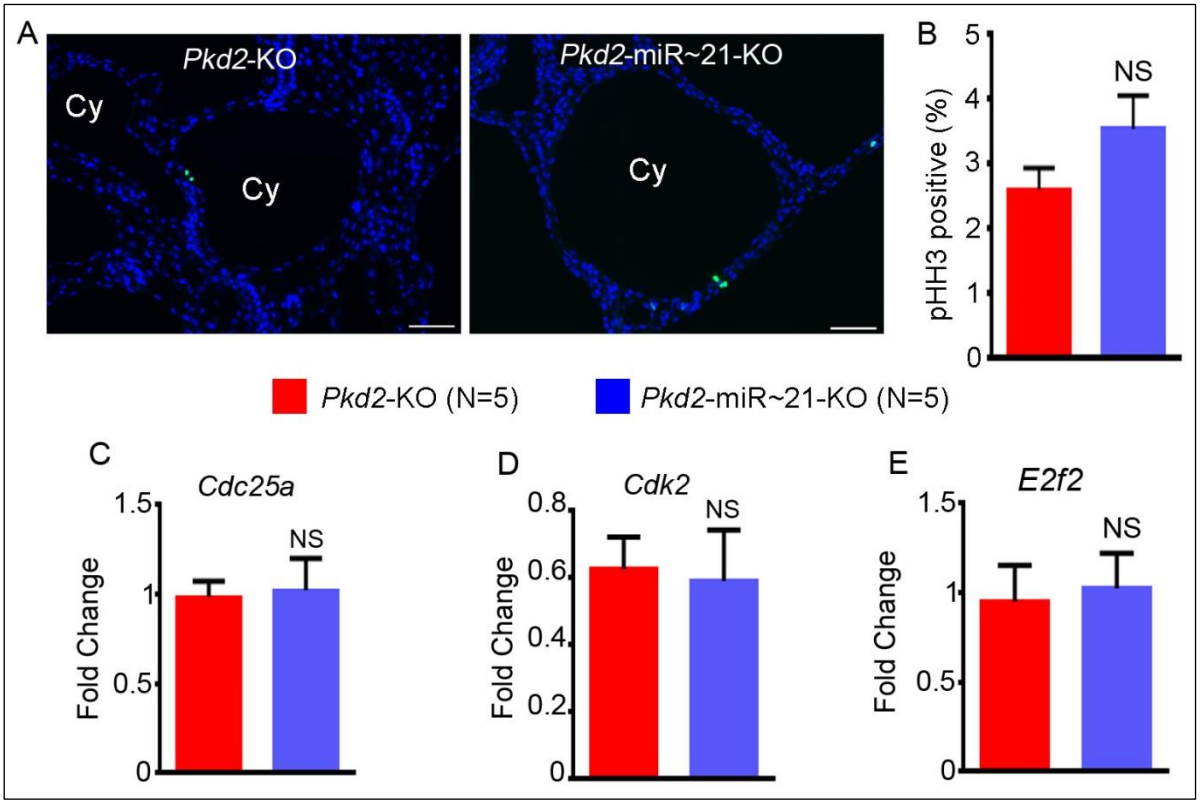

Supplementary Figure 10: Deletion of miR-21 does not affect proliferation of cyst epithelial cells. (A) Kidney sections from *Pkd2*-miR-21-KO and *Pkd2*-KO mice were stained with an antibody against Phospho-histone H3 (green, arrow) to label proliferating cells. (B) Quantification revealed no difference in the number of proliferating cyst epithelial cells between *Pkd2*-KO and *Pkd2*-miR-21-KO mice. Q-PCR analysis showed that expression of pro-proliferative miR-21 targets *Cdc25a* (C), *Cdk2* (D) and *E2f2* (E) is not different between *Pkd2*-KO and *Pkd2*-miR-21-KO mice. Cy indicates cyst, NS $P>0.05$, Scale bars = 50 µm, Error bars represent SEM.

Gene Name	log_2 fold change (DM/SM)	*P* value
Ccl1	3.07	0.0134
Fasl	1.96	0.0497
Cd69	1.25	0.0180
Dusp8	0.73	0.0015
Tspo	0.59	0.0056
Mcmdc2	0.56	0.0422
Ints6	0.55	0.0260
Med28	0.45	0.0341
Reck	0.42	0.0282

DM = *Pkd2*-miR-21-KO
SM = *Pkd2*-KO

Supplementary Table 1: List of putative miR-21 targets in cystic kidneys.